TECTONICS, VOL. 11, NO. 2, PAGES 303-315, APRIL 1992

ISOSTATIC REBOUND DUE TO TECTONIC DENUDATION: A VISCOUS FLOW MODEL OF A LAYERED LITHOSPHERE

Shimon Wdowinski[1] and Gary J. Axen
Department of Earth and Planetary Sciences, Harvard University, Cambridge, Massachusetts

Abstract. A four-layer model of the upper 150 km of the Earth is used to calculate the viscous response of continental crust and the underlying mantle to tectonic denudation. The model comprises a strong upper crustal layer, a weak lower crustal layer, a very strong mantle lithosphere layer, and a weak mantle asthenosphere layer, which is in accord with experimental constraints on strength-depth profiles for continental lithosphere. The strength of each layer is represented by its effective viscosity. Flow in the crust and mantle is driven by buoyancy forces, which arise from the unloading of an allochthon along a detachment fault by a series of instantaneous displacements (earthquakes or rapid creep events). Numerical solutions, obtained by using a finite element technique, predict footwall uplift, Moho deflection, and surface topography that are consistent with observations from the Basin and Range province of the western United States. The calculated curvature of the footwall uplift is also similar to that observed and is sensitive to the geometry of the detachment fault. Such bending need not be elastically controlled; hence the curvatures of footwall domes do not clearly place limits on the effective elastic thickness of the extending crust. The upward deflection of the Moho and the surface topography are sensitive to the viscosity structure and enable us to bound the range of the various viscosities. By matching observations from the Basin and Range province, which indicate no Moho deflection and low magnitude of surface topography ($\leq$3–5 km), we estimate the upper crustal, lower crustal, and mantle lithospheric viscosities in the ranges 10^{21}–10^{23} Pa s, 10^{19}–10^{21} Pa s, and 10^{21}–10^{23} Pa s, respectively.

INTRODUCTION

Movement on gently dipping normal faults (detachments) is an important means of accommodating continental crustal extension [Anderson, 1971; Armstrong, 1972; Wernicke, 1981; Wernicke and Burchfiel, 1982]. Such faults commonly unroof midcrustal levels, and the resulting buoyancy forces in the lithosphere cause isostatic adjustment by uplift of the footwall (Figure 1). The response of the lithosphere to this unloading provides important constraints on the mechanical behavior of continental lithosphere during extension.

Spencer [1982, 1984] and Howard et al. [1982a] proposed that isostatic rebound and doming of Cordilleran metamorphic core complexes occurred due to tectonic denudation of the crystalline cores by detachment faults that bound them. Spencer [1982] suggested that the large ratio of amplitude to diameter ($\sim$ 0.1) of the uplifted domes indicates nonelastic behavior. By assuming Airy compensation, Spencer [1984] modeled uplifts resulting from various strain distributions in the upper plate of detachment faults, reproducing observed geometries of metamorphic core complexes in the southern Basin and Range province.

Buck [1988] modeled the case in which crustal strength is bounded by a simple elastic-plastic failure envelope and extension of an elastic-plastic crustal layer above an inviscid layer is accommodated by steep normal faulting of the upper layer coupled with rapid flow of the inviscid layer. He showed, for areas of high crustal curvature where bending stresses in the elastic-plastic layer exceed the strength of crustal rocks, that the effective elastic thickness of the crust decreases to a fraction of a kilometer from the 5 km initial thickness assumed.

Block and Royden [1990] and King and Ellis [1990] modeled flexure due to extension of an elastic plate overlying an inviscid fluid. Block and Royden [1990] considered the case of detachment faulting and lateral removal of upper crustal material, and King and Ellis [1990] modeled steep normal faulting of the elastic layer. Both concluded that for elastic parameters experimentally derived for upper crustal rocks the effective elastic thickness of the upper crust must be in the range 0.5–4 km in order to produce curvatures similar to those observed in the Basin and Range province. To keep the upper crust in the elastic deformation field, King and Ellis [1990] used an effective Young's modulus that is lower than experimentally determined values by a factor of $\sim$60.

Wernicke and Axen [1988] proposed combined elastic and nonelastic behavior of the lithosphere during extension, arguing for significant elastic strength in the extending lithosphere, which supports locally uncompensated topographic loads of the Basin and Range province [e.g., Eaton et al., 1978]. They suggested that a maximum topographic load is reached, after which nonelastic responses dominate the deformation.

Block and Royden [1990] and Wernicke [1990] considered the elevations of metamorphic core complexes relative to their unextended surroundings. Both concluded that if core complexes are locally isostatically supported then the compensating fluid is of crustal density and not of mantle density.

The observations and models discussed above suggest that isostatic rebound of tectonically denuded terrains proceeds steadily through nonelastic processes over geologically measurable times (> 10,000 years), once the elastic strength of the extending lithosphere is exceeded. Ductile shear zones (mylonite zones), tens to thousands of meters thick are ubiquitous in metamorphic core complexes. These shear zones record significant ductile flow in the footwalls of detachments. Such nonelastic

[1]Now at Scripps Institution of Oceanography, La Jolla, California.

Paper number 91TC02341.
0278-7407/92/91TC-02341$10.00

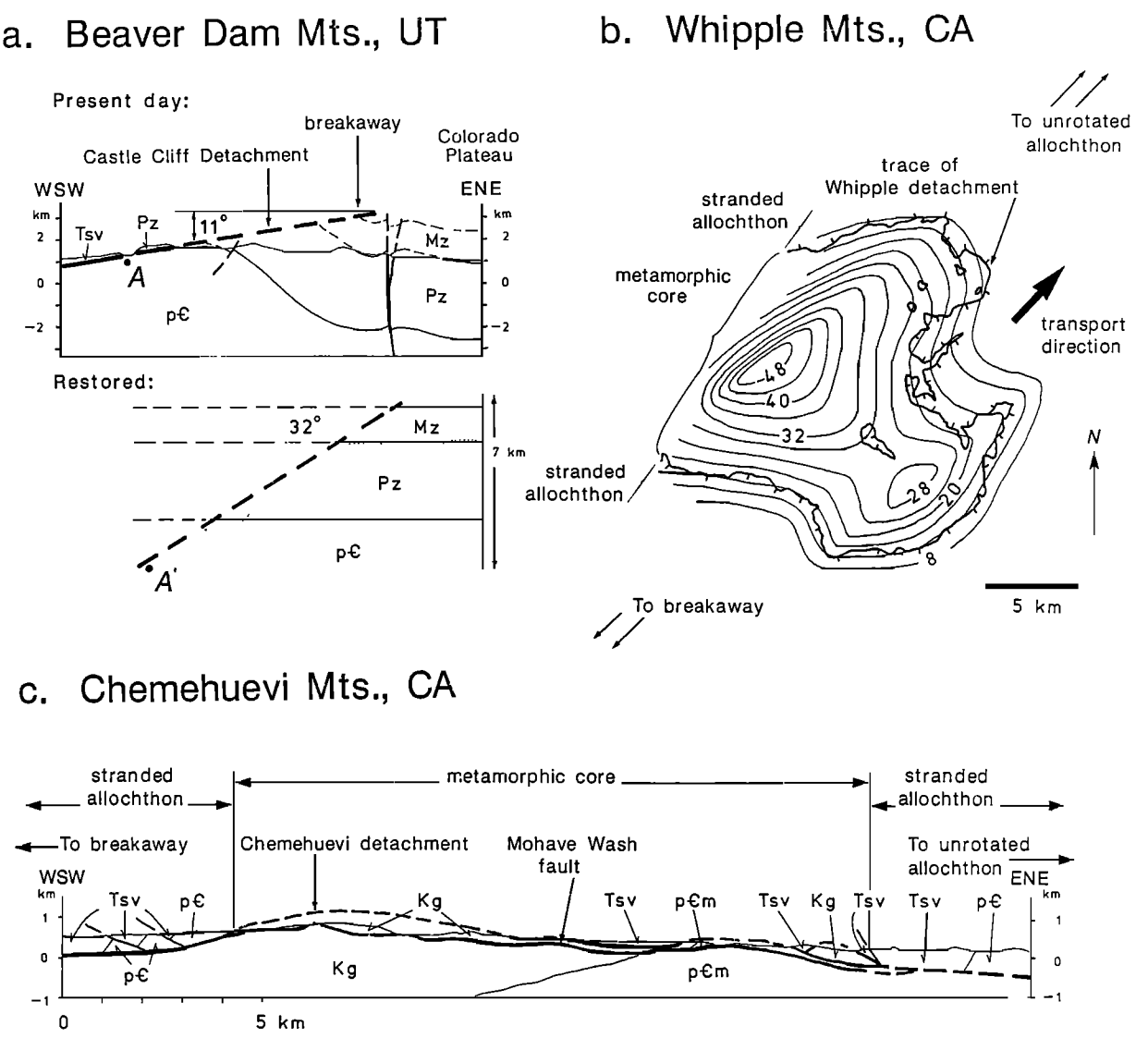

Fig. 1. Geometries of flexures and domes related to tectonic denudation. (a) Present-day and restored cross section through the breakaway zone of the Castle Cliff detachment in the Beaver Dam Mountains, Utah, at the west edge of the Colorado Plateau, showing the flexure there [after *Wernicke and Axen*, 1988]. The section is parallel to transport direction. The westernmost exposed footwall (at point A) restores to a paleodepth of 7 km (A'), indicating tectonic redistribution of at least that thickness of upper crust. About 20° of rotation of the detachment has occurred due to postdenudation uplift. (b) Structure contour map of the Whipple detachment fault (a metamorphic core complex dome) in the Whipple Mountains, California [after *Frost*, 1981]. Contours are labeled in hundreds of feet. There is about 1.2 km of relief (4000 feet) on the dome across roughly 20 km of exposure of the core. (c) Cross section of the Chemehuevi detachment system in the Chemehuevi Mountains, California [after *John*, 1987]. Section is parallel to the transport direction. The detachment is domed about 1 km across 15 km of exposure, but has been uplifted more than that amount. Upended blocks ("stranded allochthon") left behind by the migrating allochthon are up to 13 km thick measured perpendicular to the Tertiary strata [*Howard et al.*, 1982b]. This is a minimum initial depth to the detachment. Both Chemehuevi and Whipple detachment faults are rooted to the northeast, beneath the unrotated Hualapai Mountains and adjacent ranges that merge with the Colorado Plateau. Therefore Figures 1b and 1c represent only the top of much larger domical fault surfaces [e.g., *Howard et al.*, 1987, Figure 3]. Units are Tsv, Tertiary sediments and volcanic rocks; Mz, Mesozoic strata; Kg, Creteceous intrusive rocks; Pz, Paleozoic strata; p€, Precambrian crystaline rocks; and p€m, mylonitized Precambrian crystalline rocks.

processes apparently dominate much of the deformation history of metamorphic core complexes. Here we investigate a nonelastic response of the lithosphere to tectonic denudation above a detachment fault by modeling the upper 150 km of the Earth as four layers of different viscosities. Each layer in the model corresponds to a thermally and/or compositionally defined layer in the Earth.

THE MODEL

Areas that have experienced tectonic denudation, such as Cordilleran metamorphic core complexes, show significant extension of upper crustal rocks above the detachment surface. Controversy over the distribution of extension in the lower crust and mantle lithosphere centers on whether upper crustal extension is accommodated by extension of the lower crust and mantle lithosphere directly below core complexes ("in situ") [e.g., Miller et al. 1983], or whether low-angle normal faults connect regions of upper crustal extension with regions of lower crustal or mantle lithospheric extension that are laterally removed [e.g., Wernicke, 1985; Jones, 1987]. In situ mantle lithospheric extension results in net subsidence of the area that would be a metamorphic core complex, in stark contrast to the observation of relatively high-standing core complexes domes [e.g., Block and Royden, 1990]. We assume that no in situ extension occurs in deeper levels of the lithosphere; the crust and mantle respond only to unloading due to lateral removal of an allochthon in the upper crust.

The above assumption reduces the denudation problem to a relaxation problem, but not to a simple one, because the duration of the unloading (10^6–10^7 years) coincides with the time scale of lithospheric relaxation (10^5–10^6 years). As a result, the relaxation problem must be treated within the framework of the unloading process. We approach it by assuming that unloading occurs by a series of instantaneous small displacements of the allochthon that mimic deformation by earthquakes or rapid creep events in the brittle upper crust and that relaxation occurs between displacement events. The short time intervals (10^3–10^4 years) between the displacement events do not allow the crust and the mantle to reach a full relaxation during the duration of the unloading.

We consider a region of continental crust overlying mantle, with upper crustal extension accommodated by displacement of an allochthon along a detachment fault (Figure 2). The allochthon is assumed to move horizontally by a series of small instantaneous displacements. Geological studies indicate that allochthon displacements can reach a horizontal distance on the order of 50 km in a time scale of 2–10 m.y. [e.g., Reynolds and Spencer, 1985; Davis and Lister, 1988; Wernicke et al., 1989]. Detachment faults apparently dip gently (0°–30°) in the middle crust, as evidenced by seismic profiles [e.g., Allmendinger et al., 1986] and the lack of large metamorphic gradients for tens of kilometers in the direction of transport in the footwall of detachments [Crittenden et al., 1980]. In the upper crust the faults may steepen toward the breakaway fault [Howard et al., 1982a] or be gently dipping at depths of only a few kilometers [Wernicke et al., 1985, 1989; Axen et al., 1990]. In the model, we consider simple detachment fault geometries, which are characterized by two parameters: the allochthon thickness (h_0) and the detachment ramp angle (θ), which is the dip of the segment of the detachment between the surface (the breakaway) and the horizontal midcrustal part (Figure 3).

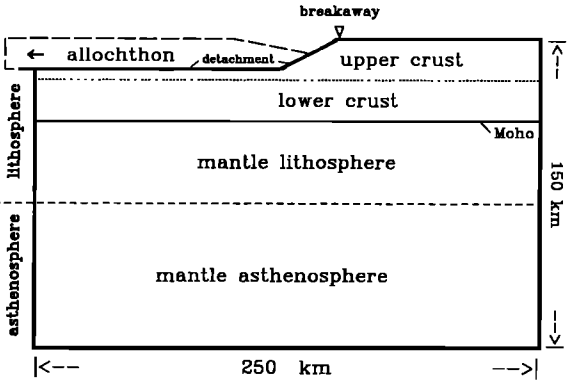

Fig. 2. Schematic diagram of the model showing a three-layer lithosphere comprised of upper crust, lower crust, and mantle lithosphere, overlying the asthenosphere, with the upper crust extending by tectonic denudation. The allochthon (long dashed lines) moves from the breakaway at a constant velocity along the detachment fault. By assuming a laterally uniform thermal gradient, the transitions between the upper and lower crust (dotted line), and between the mantle lithosphere and asthenosphere (short dashed line), which are temperature dependent, become depth dependent as well. The transition between the lower crust and the mantle lithosphere (Moho) is a compositional boundary.

Crustal response to tectonic denudation extends over a region that is wider than the denuded terrain. However, at a sufficient distance from the breakaway (100-150 km) the crust and the mantle are assumed not to respond to the unloading. Reflection seismic profiles from the northern Basin and Range province (COCORP 40°N seismic-reflection transect) show that the Moho is flat across regions with large gradients of upper crustal strain [Klemperer et al., 1986; Hauser et al., 1987], suggesting that the flow occurs mostly in the middle to lower crust. Thus we assume that the response to denudation decays with depth, and at a sufficient depth, 150 km or more, the mantle asthenosphere does not deform significantly.

The amount of deformation within the crust and mantle depends on their strength. We use a four-layer model comprising a strong upper crustal layer, a weak lower crustal layer, a very strong mantle lithosphere layer, and a weak mantle asthenosphere layer, which is in accord with experimental constraints on strength-depth profiles for continental lithosphere [e.g., Brace and Kohlstedt, 1980]. Alternation between weak and strong layers tends to concentrate the deformation within the weak layers, especially within the lower crust, because of its proximity to the denuded region. By assuming a laterally uniform geothermal gradient, the transitions

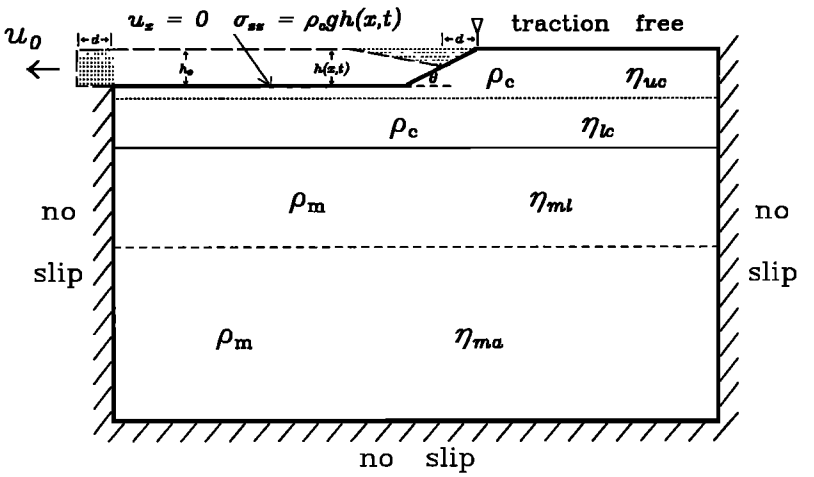

Fig. 3. Schematic diagram of the model showing the parameters and boundary conditions of the flow within the denuded lithosphere. Parameters are η_{uc}, upper crustal viscosity; η_{lc}, lower crustal viscosity; η_{ml}, mantle lithospheric viscosity; η_{ma}, mantle asthenospheric viscosity; ρ_c, crustal density; ρ_m, mantle density; d, allochthon displacement; u_0, denudation velocity; σ_{zz}, normal stress; h_0, allochthon thickness; θ, ramp angle; g, the acceleration due to gravity; and u_x, horizontal velocity. The allochthon thickness (h(x,t)) at any given time (t) and horizontal position (x) is calculated by assuming constant horizontal displacement rate of the allochthon ($d = u_0 t$) and conservation of the allochthon mass (the two dotted regions are equal in area).

between the upper and lower crust (dotted line in Figure 2), and between the mantle lithosphere and asthenosphere (short dashed line in Figure 2), which are temperature dependent, become depth dependent as well. The transition between the lower crust and the mantle lithosphere (Moho) is a compositional boundary.

Mathematical Formulation

The continental crust and the mantle are assumed to behave over long time intervals as incompressible viscous fluids. As a first approximation, we neglect along-strike variations and use two-dimensional vertical plane strain calculations. We use the plane strain formulation of Wdowinski and O'Connell [1990], which accounts for viscous and buoyancy forces. The governing equations are basically the Navier-Stokes equations (without inertial terms) that depend on the dimensionless Grashof number

$$\mathrm{Gr} = \frac{g\rho_0 x_0^2}{\eta_0 u_0} \quad (1)$$

where g is the acceleration due to gravity, and x_0, u_0, η_0, and ρ_0 are the characteristic length, velocity, viscosity, and density, respectively. The Grashof number is the ratio of buoyancy forces to viscous forces and determines the ability of a viscous fluid to respond to buoyancy forces [Turner, 1973]. It has a similar effect to that of the Argand number [England and McKenzie, 1982] in thin viscous sheet calculations. In this study, we keep g, x_0, u_0, and ρ_0 constant, and as a result Gr is a function only of the characteristic viscosity (η_0). As $\mathrm{Gr} \to 0$, corresponding to very high characteristic viscosity, the viscous fluid deforms very slowly (low velocities) in response to a given buoyancy force. As the Grashof number increases, corresponding to lower viscosity, the deformation due to the same buoyancy force is faster (higher flow velocities) and for $\mathrm{Gr} \to \infty$ (very low-viscosity), the deformation is very fast. The characteristic parameters (Table 1) yield values of the Grashof number in the range 1–1000.

Parameter Ranges

There are four types of parameters that are needed to be specified a priori: the thicknesses, the viscosities, and the densities of the the four layers (upper crust, lower crust, mantle lithosphere, and mantle asthenosphere) and the allochthon geometry (Figure 3). In order to reduce the number of free parameters, we choose to keep some of them constant throughout all calculations. Our free parameters are the viscosity structure of the four layers and the allochthon geometry. The upper and lower crust are assumed to be 20 km thick, the mantle lithosphere is assumed to be 40 km thick, and the portion of the mantle asthenosphere that is considered in the model is 70 km thick (Table 2; notice that the paremeters in Table 2 are nondimensionilized). The allochthon

TABLE 1. Values of the Characteristic Parameters That Are Used to Evaluate the Grashof Number in the Calculations

	Parameter	Value
g	gravitational acceleration	10 m s^{-2}
x_0	characteristic length	100 km
u_0	characteristic velocity	10 mm yr^{-1}
ρ_0	characteristic density	3220 kg m^{-3}
η_0	characteristic viscosity	10^{21}–10^{24} Pa s
Gr	Grashof number	0.1–1000

TABLE 2. Values of the Dimensionless Parameters Used in the Calculations.

	Parameter	Value
S_{uc}	upper crust thickness	0.2
S_{lc}	lower crustal thickness	0.2
S_{ml}	mantle lithosphere thickness	0.4
h_0	allochthon thickness	0.15
θ	detachment ramp angle	15°–45°
η_{uc}	upper crust viscosity	1
η_{lc}	lower crust viscosity	$1–10^{-3}$
η_{ml}	mantle lithosphere viscosity	1–10
η_{ma}	mantle asthenosphere viscosity	$1–10^{-3}$
ρ_c	crustal density	0.8
ρ_m	mantle density	1.0

geometry is defined by its thickness, which is assumed to be 15 km, and by the detachment ramp angle, which ranges from 15° to 45°.

The model is most sensitive to the upper crustal viscosity, which determines downward propagation of the deformation due to the unloading. If the upper crustal viscosity is very high ($\eta_{uc} \rightarrow \infty$), the upper crust will not deform in response to the unloading, and, consequently, no deformation will occur below the upper crust. Lower values of upper crustal viscosity allow deformation in the upper crust, which leads to deformation in the lower crust and mantle. We choose the upper crustal viscosity as the characteristic viscosity (η_0) and hence need to specify only the viscosity ratios, which represent the relative strengths of the layers. We are aware of no estimates of the effective viscosity of the upper crust, but by assuming that the upper crustal effective viscosity is lower than that of oceanic lithosphere and higher than that of the asthenosphere, we can bound a range of possible values. The effective viscosity of oceanic lithosphere has been estimated to be 10^{23}–10^{24} Pa s from the flexural response to long-term loads [Walcott, 1970]. The effective viscosity of the asthenosphere has been estimated from studies of postglacial rebound to be $\sim 10^{21}$ Pa s [Cathles, 1975; Peltier and Andrews, 1976]. The above estimates bound the characteristic viscosity to be in the range 10^{21}–10^{24} Pa s (Table 1). The dimensionless lower crustal viscosity (η_{lc}) and mantle asthenospheric viscosity (η_{ma}) are chosen to be in the range $1–10^{-3}$, because the lower crust and the mantle asthenosphere are weaker than the upper crust (Table 2). The dimensionless mantle lithospheric viscosity (η_{ml}), which is assumed to be stronger than the upper crust, is chosen to be in the range 1–10. For comparison, in a study of a necking instability in the Basin and Range, Zuber et al. [1986] assumed that the lower crust is 100 times weaker than the upper crust, the mantle lithosphere is twice as strong as the upper crust, and the mantle asthenosphere is 50 times weaker than the upper crust.

We consider a simple case of a buoyant crust overlying a denser mantle; the crustal density (ρ_c) is assumed to be 20% less than the mantle density (ρ_m) (2670 kg m^{-3} versus 3320 kg m^{-3} [Block and Royden, 1991]). Buoyancy forces are dominated by the upper surface topography, which changes during the allochthon displacement. Hence small density variations (< 5%) lower in the crust are negligible and are omitted from the model.

Boundary Conditions

In this study, we investigate the crustal and mantle response to tectonic denudation caused by extension of the upper crust; the lower crust and the mantle are assumed to deform only in response to the unloading in the upper crust. In addition, we assume that tectonic denudation is a local phenomenon and that at a sufficient distance from the breakaway (100–150 km), the crust and the mantle do not respond to the unloading. Thus we impose a condition of no slip along the vertical and the bottom boundaries (Figure 3).

Although the Earth's surface is a traction-free boundary, the detachment surface beneath the allochthon, which is excluded from our calculations, is subjected to tractions. We impose the allochthon load, as a normal stress boundary condition along the detachment fault. The normal stress ($\sigma_{zz}(x,t) = \rho_c g h(x,t)$) is proportional to the height of the allochthon (h), where the height of the allochthon is a function of horizontal position (x) and time (t) (see below). This implicitly assumes negligible flexural strength for the allochthon. The allochthon is assumed to move by a series of instantaneous displacements (earthquakes or creep events), without displacing the detachment surface. This is in accord with our assumption that below the detachment surface the crust and the mantle respond only to the unloading, without experiencing in situ extension. Thus along the detachment surface we impose zero horizontal velocity and a condition on the normal stress (σ_{zz}), which allows this surface to move vertically and to sustain tractions. Elsewhere along the upper boundary we impose traction-free boundary conditions.

Method of Solution

We use a finite element technique with eight-noded quadrilateral isoparametric elements to solve numerically for the velocity field. In addition, a penalty function formulation is used to replace the pressure term for incompressibile fluid and solved by a selective reduced integration technique [Zienkiewicz, 1977]. We conducted various numerical experiments with 200-800 elements and 100-400 time steps to ensure that the solutions are grid- and time-step independent. As well, various patch tests have been conducted to ensure that the code is free of zero-energy and propagating spurious modes [Zienkiewicz, 1988]. Because the governing equation is time-independent, we solve for the velocity field at successive time steps. At the initial stage the allochthon has not been displaced, the buoyancy forces are zero, and there is no flow within the lithosphere. The allochthon is assumed to move by a series of instantaneous displacements. We introduce the unloading by changing the vertical stress boundary conditions ($\sigma_{zz}(x,t)$), which would arise from horizontal displacement of the allochthon, along the detachment surface. The stress

boundary condition at any given time and horizontal position ($\sigma_{zz}(x,t)$) is calculated by assuming a constant horizontal displacement rate of the allochthon and conservation of the allochthon mass. These assumptions correspond to the end member case of an internally unextended allochthon. Mathematically, the stress is calculated by assuming that the two dotted regions in Figure 3 are equal in area; the area of the dotted rectangle ($d \times h_0$) and the height of the dotted triangle ($d \times \tan\theta$) determine the length of the triangle ($2h_0/\tan\theta$) (or of the trapezoid in later stages of the denudation). The velocity field within the crust and the mantle, due to the unloading, is calculated for each time step. In order to calculate the element grid of the next time step, we assume constant velocity between two successive time steps. This assumption is valid for small time steps in which the time increment between steps is smaller than 50,000 years. We use 200–400 time steps to calculate the lithospheric and asthenospheric response to a denudational event occurring during 2–6 Ma.

RESULTS

Figure 4 shows the velocity field that is generated within the crust and mantle in response to tectonic denudation. The general flow pattern is upwelling beneath the breakaway and downwelling between the breakaway and the side boundaries. This results from the no-slip boundary conditions along the side and bottom boundaries, which enforce the subsidence of the upper surface near the side boundaries in order to conserve the uplifted mass near the breakaway. The magnitude of the flow velocity depends on the lateral extent of the denuded region and on the Grashof number (Gr), which determines the ability of the viscous fluid to respond to buoyancy forces. The velocity of the flow decreases with depth where the velocity gradient is dependent on the vertical viscosity structure. A very high viscosity layer (almost rigid), which reduces or may even halt the downward propagation of the deformation, can decrease significantly the flow in that layer and below it. In

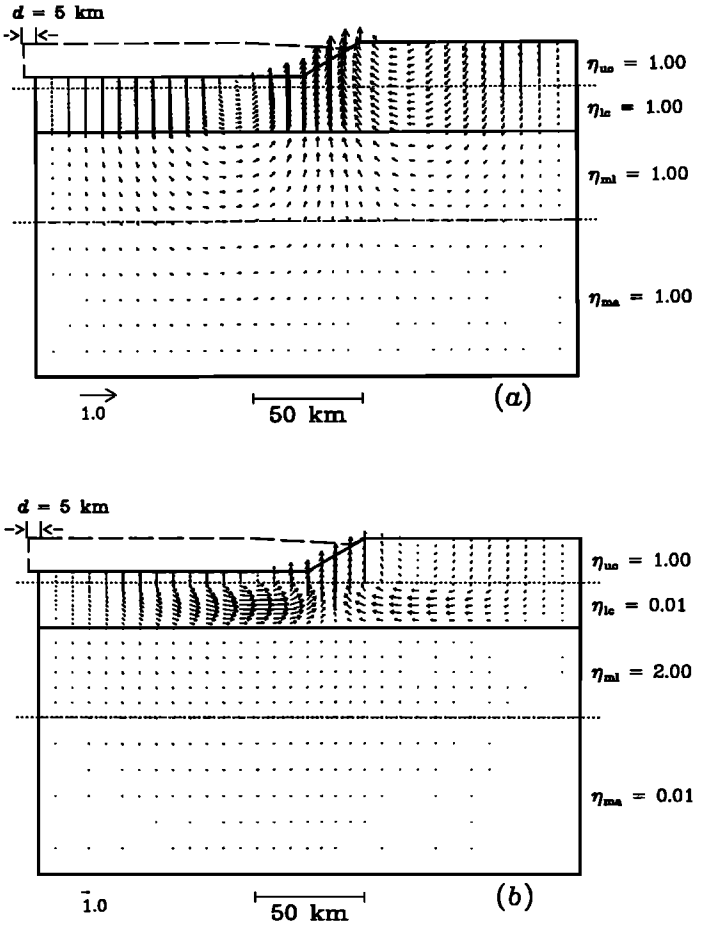

Fig. 4. The flow field within the crust and mantle in response to tectonic denudation. The velocity scale is given by the arrow below the lower left corner, which is scaled to the characteristic velocity (u_0). (a) Velocity field for a constant viscosity (Gr = 500, $\eta_{uc} = \eta_{lc} = \eta_{ml} = \eta_{ma} = 1$). The mantle participates in the overall flow. (b) Velocity field for a more realistic viscosity structure ((Gr = 500, $\eta_{uc} = 1$; $\eta_{lc} = 0.01$; $\eta_{ml} = 2$; $\eta_{ma} = 0.01$). The flow is concentrated within the crust and forms a low-viscosity channel flow.

contrast, a low-viscosity layer, which accommodates most of the deformation, tends to amplify the flow in the layer; the magnitude of the flow increases with lower viscosity values.

For depth-invariant viscosity (Figure 4a), the vertical velocity gradient is small and the mantle participates in the overall flow. For a possibly more realistic viscosity structure, where the lower crustal and mantle asthenospheric viscosities are 2 orders of magnitude less than the upper crustal and mantle lithospheric viscosities (Figure 4b), the flow field is confined to the crust, with negligible flow in the mantle. By generating a channel flow in the low-viscosity lower crust, rather than by deforming the strong mantle lithosphere, the lower crust moves more effectively into the denuded area. Similarly, if the mantle lithosphere is almost rigid (very high viscosity) the unloading affects only the crust. The low-viscosity of the mantle asthenosphere has no influence on the flow, because most of the flow is concentrated within the crust, and the very strong mantle lithosphere does not transmit deviatoric stress downward.

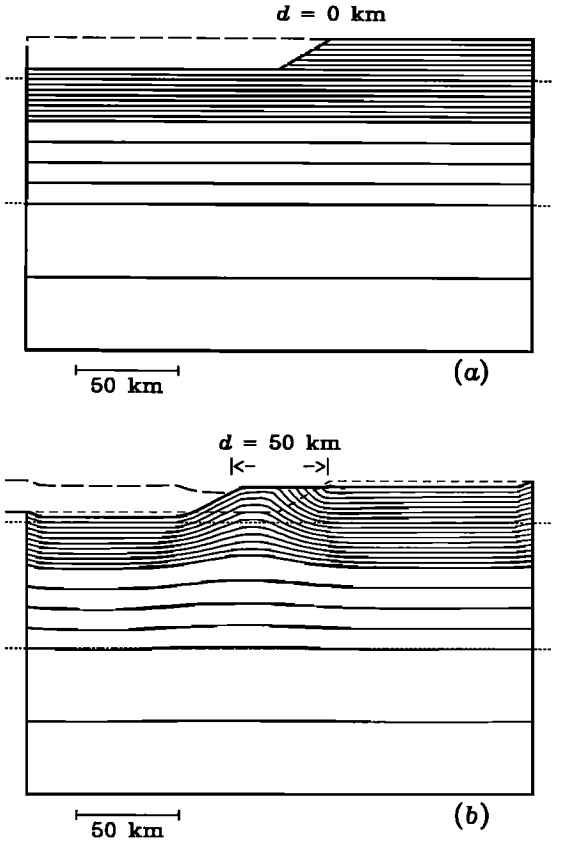

Fig. 5. Simulation of geometrical relations between rock units (with $u_0 = 1.0$, Gr = 500, $\eta_{uc} = 1$, $\eta_{lc} = 0.01$, $\eta_{ml} = 2$, $\eta_{ma} = 0.01$). (a) At the initial stage, the undeformed horizontal markers are 2.5 km apart. (b) After 50 km of allochthon displacement, during 5 m.y. (calculated in 250 time steps). The short dashed line indicates the original shape of the detachment. The markers are deformed and show footwall uplift, Moho deflection, and surface topography.

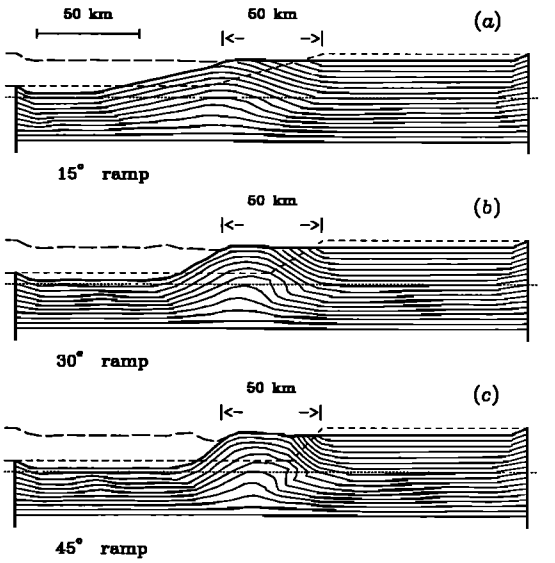

Fig. 6. Simulation of geometrical relations in the crust for various detachment geometries after 50 km of allochthon displacement. The time-stepping procedure is the same as for Figure 5, with $u_0 = 1.0$, Gr = 500, $\eta_{uc} = 1$, $\eta_{lc} = 0.01$, $\eta_{ml} = 2$, $\eta_{ma} = 0.01$. The detachment ramp dips (a) at 15°, (b) at 30°, and (c) at 45°. See text for discussion.

We try to simulate observed geometrical relations between various rock units (Figure 1) by tracing the shapes of marker that initially are horizontal (Figure 5a). Figure 5b shows an example of these markers after being deformed in response to 50 km of allochthon displacement during 5 m.y. (calculated in 250 time steps). The isostatic rebound in response to the unloading causes crustal uplift beneath the denuded allochthon and subsidence of the upper and the detachment surfaces in order to conserve the uplifted mass. Horizontal markers that were initially located beneath the allochthon (at depth of 15 km) are uplifted to the surface and form a dome-shaped structure similar to that of metamorphic core complex domes (Figure 1). Although the two-dimensional formulation indicates a cylindrical structure, the term dome is used because of the similarity to the observed metamorphic domes. The dome geometry is determined by the allochthon thickness (h_0) and the horizontal displacement (d); the allochthon thickness determines the amplitude of the dome, and the displacement determines the diameter (wavelength) of the dome. There are three important geometrical features that are produced by the model: flexure and footwall uplift near the breakaway, Moho deflection, and surface topography.

Figure 6 shows that for a given viscosity structure, various curvatures of the uplifted footwall are produced with various detachment geometries. Furthermore, for a given detachment geometry the curvature of the uplifted footwall changes little for a large range of the other parameters (Figures 7 and 8). Thus the geometry of the flexure is sensitive to the detachment geometry but relatively insensitive to the strength of the various layers.

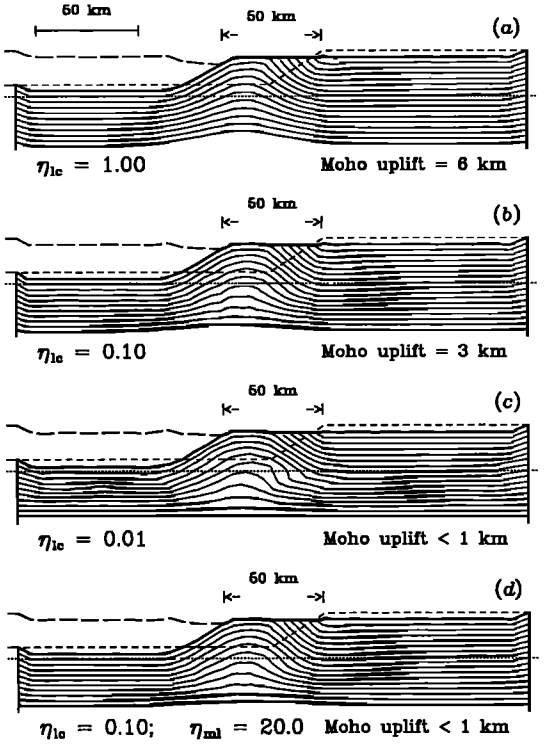

Fig. 7. Calculations of Moho deflection as a function of the dimensionless lower crustal viscosity (η_{lc}) with other parameters held constant ($u_0 = 1.0$, Gr = 500, $\eta_{uc} = 1$; $\eta_{ml} = 2$; $\eta_{ma} = 0.01$). The time stepping procedure is the same as for Figure 5. (a) $\eta_{lc} = 1.0$, (b) $\eta_{lc} = 0.1$, (c) $\eta_{lc} = 0.01$, and (d) $\eta_{lc} = 0.1$ and $\eta_{ml} = 20$. Moho uplift is measured between the highest and lowest point on the Moho. See text for discussion.

The results compare favorably with several footwall uplifts in the Basin and Range province in terms of amplitude, curvature, and wavelength of the synformal part near the breakaway (Figure 1a and Wernicke and Axen [1988, Figures 2 and 3]).

In contrast, the Moho deflection and the topography are sensitive to the viscosity structure and to the Grashof number, which enables us to place bounds on some of these parameters. The upward deflection of the Moho is caused by an upwelling flow within the mantle, beneath the breakaway. As shown in Figure 4, the magnitude of flow in the mantle is controlled by the lower crustal and mantle lithospheric viscosities. When the lower crustal viscosity is the same as the upper crustal and mantle lithospheric viscosities, the mantle participates in the overall flow, and the Moho is deflected upward (Figure 7a). The amplitude of the deflection decreases as the lower crustal viscosity decreases (Figures 7b and 7c), or as the mantle lithospheric viscosity increases (Figure 7d). For both detachment geometry and Grashof number held constant, the amplitude of Moho deflection is determined by the ratio between the lower crustal and the mantle lithospheric viscosities. When this ratio is lower than 0.01 (for Gr in the range 100–1000) the amplitude of the deflection is very low (< 1 km), and below that value the amplitude is practically zero.

Our model assumes that the crust and the mantle behave over long periods of time as viscous fluids. Any topographic relief that is not dynamically supported will decay with a sufficient amount of time. However, during the finite period of time of a denudation event the crust and mantle cannot fully relax, allowing some relief to exist. The short-wavelength (up to about 20 km) relief follows the shape of the denuded allochthon. The long-wavelength relief (50-100 km) is supported by the flow field that is induced by the denuded allochthon and has a dome shape that is centered around the topographic low next to the detachment at the surface. This may cause the metamorphic core and nearby areas to have higher elevations than their surroundings (Figure 6). Detachment geometry determines the short wavelength surface relief, but can also affect long wavelength relief, because it determines the size and the distribution of buoyancy forces; in terms of the model it determines the magnitude and distribution of the stress boundary conditions. For a given detachment geometry, the magnitude of the relief depends mostly on the Grashof number (Gr), which determines the relaxation time of the upper crust. However, the relief can vary significantly during the early stages of a denudation event, when the wavelength of the relief is too short to

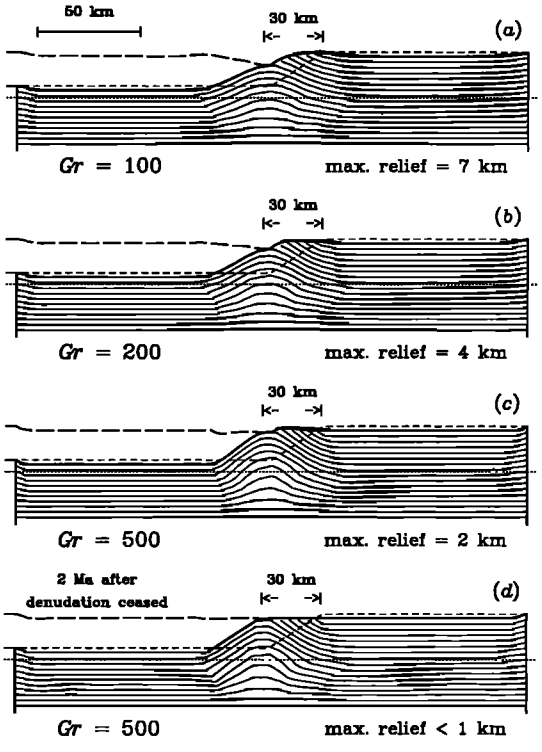

Fig. 8. Calculations of surface relief as a function of the Grashof number (Gr) after 30 km of allochthon displacement, during 3 m.y. (calculated in 300 time steps); the other parameters are held constant ($u_0 = 1.0$, $\eta_{uc} = 1$; $\eta_{lc} = 0.01$; $\eta_{ml} = 2$; $\eta_{ma} = 0.01$). (a) Gr = 100, (b) Gr = 200, (c) Gr = 500, and (d) no surface relief, 2 Ma after the denudation ceased (with Gr = 500).

have any significant effect on the viscous forces. In later stages, when the wavelength of the denuded region is longer, the relief is determined by the Grashof number. Figure 8 shows examples of surface topography after 30 km of allochthon displacement, as a function of the Grashof number (calculated in the same way as Figure 5). For Gr = 100 the maximum relief reaches 4 km (Figure 8a), whereas for Gr = 500 the maximum relief is lower and reaches only 2 km (Figure 8c). After denudation ceases, the modeled lithosphere can fully relax (in 1–2 m.y.), flattening the surface relief but preserving the geometry of the uplifted footwall dome (Figure 8d).

DISCUSSION

Several aspects of this model agree well with geometries observed in areas where large-magnitude upper crustal extension has been concentrated on low-angle normal faults. The model reproduces the curvature and uplift observed in detachment terrains (e.g., Figure 6) without elastic flexure of the crust. Therefore elastic behavior need not have played an important role in the formation of such uplifts, as postulated by Wernicke and Axen [1988]. This agrees well with elastic flexure models that require the bulk of the crust in such areas (all but a fraction of a kilometer) to have behaved nonelastically in order to reconcile the magnitudes of fiber stresses with the strength of crustal materials [Buck, 1988; Block and Royden, 1990, King and Ellis, 1990].

The topographic relief produced by our model would be ephemeral if the crust were truly viscous. However, the upper crust clearly has a substantial elastic thickness even when in extension, as indicated by normal-fault earthquake foci to depths of 10-15 km [e.g., Jackson, 1987] and by locally uncompensated topography [e.g., Eaton et al., 1978]. Effective elastic thickness deduced from the curvature of footwall domes (i.e., the part of flexed crust in which strength is greater than fiber stresses) does not represent the the thickness of the upper crust that elastically supports such topographic loads [e.g., Wernicke and Axen, 1988]. Because the boundary between upper and lower crust is principally a thermal one, viscously upwelling lower crust is in effect transferred to the upper crust if cooling is rapid relative to uplift. In that case the thickness of the upper crustal layer that stores the elastic stress released in earthquakes (our high-viscosity upper crust) need not be substantially changed and may support topographic relief produced through nonelastic mechanisms.

Such an effect may be represented by the western edge of the Colorado Plateau, where a topographic high of 0.3–1.0 km above the regional plateau elevations is parallel to the breakaway zone [Wernicke, 1985]. Locally this relief is spatially coincident with a large-scale fold, but elsewhere uplift was accommodated largely by subvertical faults [Moore, 1972; Wernicke and Axen, 1988]. These faults are large enough (to ~ 4 km offset) that they probably penetrated through the entire strong upper crustal layer. Such breakaway-side-down shear is consistent with the strain path predicted by our model (Figure 9; see discussion below and Axen and Wernicke [1991]).

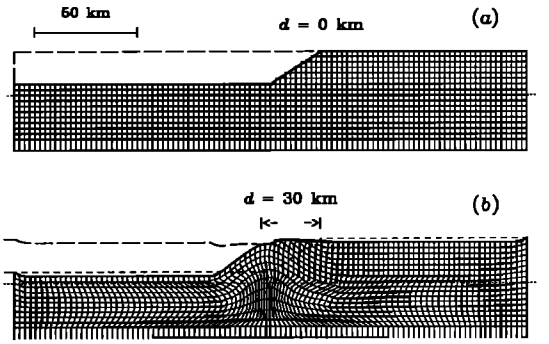

Fig. 9. Finite strain in the footwall of the detachment. (a) Before deformation each square is 2.5 × 2.5 km^2. (b) After 30 km of allochthon displacement, during 3 m.y. (calculated in 300 time steps) the squares are deformed. Notice that near the breakaway the surface squares have experienced breakaway-side-down simple shear along vertical planes.

The geometry of the synform near the breakaway is largely a function of the geometry of the detachment fault there (see previous section and Figure 6). Curvature and final dip of initially horizontal markers in the breakaway synform increase with initial dip of the detachment ramp. This agrees with footwall geometries observed in the Mormon Mountains region below detachments that had different initial dips, and where initially subhorizontal layering is present [Axen et al., 1990].

In metamorphic core complexes it is generally impossible to recognize initially horizontal markers like those in Figure 6, making the strain pattern shown there difficult to apply directly. The dome typically is defined by mylonitic foliation that may have formed in a dipping shear zone. For example, the last mylonites probably form parallel to the base of the detachment ramp in the ductile midcrustal. Such initially dipping markers will record a different strain path than originally horizontal ones [e.g., Axen and Wernicke, 1991].

Seismic reflection profiles in the Basin and Range province show a relatively flat, featureless Moho [Klemperer et al., 1986; Hauser et al., 1987]. This occurs in our model when the ratio of lower crustal to mantle lithospheric viscosities is less than 0.01, causing Moho uplift over a broad area in response to local unroofing. Although Moho uplift is minor in our models (0–7 km), this is mostly due to the modest amount of extension: 50 km in 250 km length, or 20% extension. Much larger amounts of extension have been documented regionally (e.g., 200–500% in the Basin and Range province near Las Vegas, Nevada [Wernicke et al., 1988]). Flow in the middle to lower crust may be an important mechanism for coupling upper crustal extensional strain with uplift of the upper mantle.

Relief on the Moho is also minimized by local shortening and thickening of lower and middle crust below denuded terrains (Figure 9). This is important in deeply eroded regions, where such a zone may be mistakenly interpreted as an evidence of continental orogeny.

The model predicts geometrical relations such as

footwall uplift, Moho deflection and surface topography, which can be compared with the observations and used to bound the range of the free parameters. First we estimate the characteristic viscosity by evaluating the range of possible values of the Grashof number. Topographic relief created in our viscous flow model of the crust during a denudation event would decay rapidly after cessation of movement on the detachment (in 1–2 m.y.).

In actively extending areas of the Basin and Range province, such as around Death Valley, the maximum relief is about 3 km, with regionally averaged topographic relief more typically in the range 1–1.5 km. Here we neglect effects of erosion and of the load due to density differences between basin fill and bedrock, which has the same effect as slightly increasing loads due to topographic relief. The sensitivity of the topography to the Grashof number determines Gr in the range 100–1000, which will support maximum topography of about 3 km throughout the entire time-stepping calculations, depending on the detachment geometry. In our formulation the Grashof number is a function only of the characteristic viscosity because all the other characteristic parameters are fixed. Thus Gr in the range 100–1000 yields an upper bound of 10^{21}–10^{22} Pa s for the characteristic viscosity, which is the effective viscosity of the upper crust. As shown in Figure 4, the lower crustal viscosity determines the lower crustal velocity field. By assuming that the velocity of flow in the lower crust cannot exceed more than 10 cm/yr, which is 10 times faster than the unloading rate, we estimate the lower crustal viscosity to be 10–100 times lower than the upper crustal viscosity. Thus our lower crustal viscosity estimate is 10^{19}–10^{21} Pa s. Our estimate agrees with that of Kruse et al. [1991], who estimated the effective viscosity of the lower crust to be 10^{18}–10^{20} Pa s in the Colorado Plateau adjacent to the Basin and Range province. For a shorter length scale of channel flow (150 km) the viscosity can be higher, about 10^{21} Pa s [Kruse et al., 1991]. Figure 7 shows that no Moho deflection occurs when the ratio of lower crustal to mantle lithospheric viscosities is lower than 0.01; thus we estimate the viscosity of the mantle lithosphere to be in the range 10^{21}–10^{23} Pa s. We cannot estimate the mantle asthenospheric viscosity because our model is not sensitive to this parameter. The average strength of the lithosphere is predominantly determined by the strength of the very strong mantle lithosphere [England and McKenzie, 1982]. This suggests that the effective lithospheric viscosity should be 10^{21}–10^{23} Pa s. Indeed, England [1986] argued that the average viscosity of the lithosphere might need to be as low as 10^{22} Pa s for extensional regions to deform as rapidly as they do.

The various models predict finite-strain geometries and strain histories that can be compared with field observations. For elastically controlled flexural failure models [e.g., Buck, 1988; King and Ellis, 1990] layer-parallel shortening and elongation are predicted for the concave and convex areas of flexures, respectively. This is complicated near the allochthon because the footwall there is first bent and then unbent, and discussion of the strain path followed by such an elastically flexing footwall is beyond the scope of this paper [see Axen and Wernicke, 1991]. Figure 9 shows a grid that is initially formed of 2.5 km by 2.5 km squares. After 30 km of allochthon displacement in 3 m.y., the grid has been deformed, and each quadrilateral represents the net local finite strain. Near the breakaway, the finite strain in the footwall is principally represented by breakaway-side-down subvertical simple shear. Breakaway-side-down faulting is almost ubiquitous along the western margin of the Colorado Plateau on faults from outcrop to map scale with displacements measured in millimeters to kilometers [e.g., Moore, 1972; Smith et al., 1987; Wernicke and Axen, 1988], and agrees well with the above result. Bartley et al. [1990] showed that the strain path followed by the footwall of the central Mojave metamorphic core complex is consistent with a flexural failure mechanism of uplift, akin to that modeled by Buck [1988]. However, ambiguities exist which also allow for an interpretation in which distributed subvertical simple shear accounts for the strain path [Axen and Wernicke, 1991]. For example, much of the footwall uplift there apparently occurred along subvertical hanging-wall-side-up structures [Bartley et al., 1990], consistent with the latter interpretation.

The finite strain of the denuded footwall near the allochthon (Figure 9) is somewhat difficult to apply due to the lack of appropriate strain markers there. For example, the unroofed grid elements directly adjacent to the allochthon (Figure 9b) are nearly square, implying little net finite strain. In fact, these elements have experienced (1) early hanging-wall-side-down subvertical simple shear as they passed out from under the base of the hanging wall ramp, then (2) hanging-wall-side-up subvertical simple shear, as they passed out from under the hanging wall. The earlier strain history (1) would likely be obliterated by subsequent mylonitization as the footwall is translated up the deeper (ductile) part of the ramp. Hence the strain markers most suitable for recording the the second strain event (2) would be initially dipping mylonites. See Axen and Wernicke [1991] for further discussion.

LIMITATION OF THE MODEL

This simple model ignores along-strike variations and assumes two-dimensional flow. However, the domal structure of denuded footwalls suggests that three-dimensional geometry and flow are important. It is possible that the transport-parallel warping of detachment surfaces (e.g., Figure 1a) is due to variations along strike in thickness of the allochthon, rather than later folding or an initially broadly corrugated fault surface. At present, a three-dimensional model is difficult to formulate because the geometry, boundary conditions, and various parameters (viscosity and density structure) are poorly constrained. Investigations of two-dimensional models can impose some constraints on the problem, which will help to constrain future investigations of more realistic three-dimensional models.

Here we model the process of flow in the middle and lower crust acting in response to tectonic denudation, rather than attempt a formulation that represents the crust itself and the wide variety of deformation mechanisms that may be in play. The continental lithosphere deforms by various processes, such as, brittle failure, power-law creep, and cataclastic flow. Other

studies of continental deformation have assumed that the lithosphere behaves as perfectly plastic material [e.g., Tapponier and Molnar, 1976], as a viscoelastic material [e.g., Vilotte et al., 1986], or as a power law fluid [e.g., England and McKenzie, 1982]. In our calculations, we assume that the crust and the mantle behave over long period of time as Newtonian fluids, which significantly simplifies the model and the calculations. Kruse et al. [1991] show that linear viscous rheology satisfactorily approximates deformation by power law creep in the case of channelized flow, as modeled here for the weak lower crust. Therefore the linear viscous flow assumption need not necessarily correspond to any specific deformation mechanism in order to relate the rate and locus of deformation to the stresses derived from tectonic unroofing. The effective viscosities represent average strengths of each of the four layers, each of which deforms by the various mechanisms (e.g., brittle failure, creep, and cataclastic flow).

Temperature variations, which are neglected in the model, mostly affect the strength of rocks. We have taken into account the first-order effect of the temperature by separating the upper 150 km of the Earth into strong and weak layers. Lateral temperature variations, which are second-order effects, may change the shape of the layers, or locally affect the strength of rocks, but should not change the general results. Calculations with more realistic and less simplistic constitutive relations will probably produce somewhat different results and should be approached in future studies.

Although the model creates topography during the deformation event, the topography decays rapidly after cessation of movement on the detachment (in 1–2 m.y.). Long-lived topography in areas where rapid extension ceased 10 m.y. or more ago (e.g., Whipple Mountains, [Davis and Lister, 1988], Nopah and Resting Spring ranges [Wernicke et al., 1989] suggests that the crust has significant elastic strength and that this strength supports the topographic loads. In the real world, the viscous response of the lithosphere to the unloading is stress dependent. Thus during a denudation event, when the stresses are high, the deformation and the topography are dominated by the viscous behavior of the crust. After cessation of denudation the stresses decrease, and elastic behavior dominates the crustal deformation. Visco-elastic constitutive relations may be more suitable for the purpose of explaining topography. However, viscoelastic relations demand specifying additional free parameters which will complicate the model.

In order to keep a simple time-stepping procedure, the allochthon and sedimentary basin loads were excluded from our calculations. We considered only the allochthon load and ignored any strength or deformation within the allochthon. In reality, deformation within the allochthon changes the load distribution, but this is not expected to be a first-order effect [cf. Spencer, 1984]. Internal extension of the hanging wall leeds to asymmetrical arch, with gentler dips on the hanging wall side. The allochthon is probably divided into two strength domains: the unextended part probably has strength similar to the bulk of the upper crust, and the extended part may account for little strength. Similarly, the effects of basin-fill loads need to be analyzed, although this is probably not a first-order effect (e.g., compare the results of Buck [1988] for experiments with and without sedimentation). Future models should address the strength as well as the load of the allochthon and sediments.

In the model, extension is limited to the upper crust, whereas the lower crust and mantle deform only in response to the unloading. This is in accord with the small amount of the overall subsidence observed in metamorphic core complexes and contrasts with the much larger amounts of subsidence that would be expected if in situ mantle extension occurred [White and McKenzie, 1988]. We feel that the bulk of the data indicates that the locus of mantle lithospheric extension related to metamorphic core complex formation is laterally removed from the denuded terrains in the upper crust [e.g., Wernicke, 1985; Jones, 1987]. However, examples exist in which in situ mantle extension is indicated (e.g., the Rio Grande Rift [Olsen et al., 1979; Prodehl and Lipman, 1989]). Future modeling should consider this scenario also.

In our model, as well as those of Buck [1988], Block and Royden [1990], and King and Ellis [1990], footwall uplift is accommodated entirely by bending. Although this may be the case in a number of places, it also appears that uplift can be accommodated along discrete zones of failure (such as steep faults), as was apparently the case in the North Virgin Mountains [e.g., Wernicke and Axen, 1988]. This implies that the mechanical spectrum of footwall response to tectonic denudation is broader than has been considered to date in continuum modeling. Such responses should be considered in future studies.

CONCLUSIONS

A four-layer model of the upper 150 km of the Earth is used to calculate the viscous response of continental crust and the underlying mantle to tectonic denudation. The model comprises a strong upper crustal layer, a weak lower crustal layer, a very strong mantle lithosphere layer, and a weak mantle asthenosphere layer, which is in accord with experimental constraints on strength-depth profiles for continental lithosphere. The strength of each layer is represented by its effective viscosity. The flow in the crust and mantle is driven by buoyancy forces, which arise from the unloading of an allochthon along a detachment fault by a series of instantaneous displacements (earthquakes or rapid creep events).

Numerical solutions, obtained by using a finite element technique, predict footwall uplift, Moho deflection, and surface topography. The curvature of the footwall uplift is similar to that which has been observed in regions that experience tectonic denudation (e.g., the Basin and Range province), and is determined by the geometry of the detachment fault. The upward deflection of the Moho and the surface topography are sensitive to the viscosity structure and enable us to bound the range of the various viscosities. By matching observations from the Basin and Range province, which indicate little Moho deflection and low magnitude of surface topography ($\lesssim$3–5 km), we estimate the upper crustal, lower crustal, and mantle lithospheric viscosities in the ranges 10^{21}–10^{23} Pa s,

10^{19}–10^{21} Pa s, and 10^{21}–10^{23} Pa s, respectively.

Melosh [1990] showed that extension of an elastic layer overlying a viscous layer could result in initial detachment geometries similar to those modeled here: a steeper portion that transects the strong, upper crustal layer, and a flat portion at depth where strength has decreased. Although our model does not include elastic strength of the upper crustal layer, it does account well for deformation that would be expected after the elastic limit of the upper crust has been reached. More comprehensive viscoelastic models seem to be required, in order to reproduce initial fault trajectories, deformation histories, and resulting topography.

An important feature of any model of lithospheric behavior is that it be testable. The models presented here suggest strain histories and strain states in the upper crust that locally differ from those that would be produced, for example, by elastically controlled flexure, such as that proposed by Buck [1988] (see also Axen and Wernicke [1991]). Field studies in appropriately chosen areas should be able to provide these tests.

Acknowledgments. This work was supported by NASA grant NAG5-840, and NSF grant EAR-8903912 awarded to R. J. O'Connell, and NSF grants EAR 8451181 and EAR 8917227 awarded to B.P. Wernicke. Axen's salary was provided by the NSF Graduate Fellowship Program. We thank Leslie Sonder and Roger Buck for helpful reviews. We gratefully acknowledge helpful discussions with John Bartley, Bruce Buffett, Richard J. O'Connell, Mark Linker, J. K. Snow, Joann Stock, and Brian P. Wernicke.

REFERENCES

Allmendinger, R. W., H. Farmer, E. Houser, J. Sharp, D. Von Tish, J. Oliver, and S. Kaufman, Phanerozoic tectonics of the Basin and Range-Colorado Plateau from COCORP data and geologic data: a review, in *Reflection Seismology: The Continental Crust, Geodyn. Ser.*, vol. 14, edited by M. Barazangi and L. Brown, pp. 257-267, AGU, Washington, DC., 1986.

Anderson, R. E., Thin-skin distension in Tertiary rocks of southeastern Nevada, *Geol. Soc. Am. Bull., 82*, 43-58, 1971.

Armstrong, R. L., Low angle (denudation) faults, hinterland of the Sevier orogenic belt, eastern Nevada and western Utah, *Geol. Soc. Am. Bull., 83*, 1729-1754, 1972.

Axen, G. J., and B. Wernicke, Comment on "Tertiary extension and contraction of lower-plate rocks in the central Mojave metamorphic core complex, Southern California", by John M. Bartley, John M. Fletcher, and Allen F. Glazner, *Tectonics, 10*, 1084-1086, 1991.

Axen, G. J., B. Wernicke, M. F. Skelly, and W. J. Taylor, Mesozoic and Cenozoic tectonics of the Sevier thrust belt in the Virgin River Valley area, southern Nevada, in Basin and Range Extensional Tectonics Near the Latitude of Las Vegas, Nevada, edited by B. Wernicke, *Mem. Geol. Soc. Am., 176*, 123-153, 1990.

Bartley, J. M., J. M. Fletcher, and A. F. Glazner, Tertiary extension and contraction of lower-plate rocks in the central Mojave metamorphic core complex, Southern California, *Tectonics, 9*, 521-534, 1990.

Block, L., and L. Royden, Core complex geometries and regional scale flow in the lower crust, *Tectonics, 9*, 557-567, 1990.

Brace, W. F., and D. L. Kohlstedt, Limits on lithospheric stress imposed by labratory experiments, *J. Geophys. Res., 85*, 6248-6252, 1980.

Buck, W. R., Flexural rotation of normal faults, *Tectonics, 7*, 959-973, 1988.

Cathles, L. M., *The Viscosity of the Earth's Mantle*, Princeton University Press, Princeton, N. J., 1975.

Crittenden, M. D., P. J. Coney, and G. H. Davis (Eds.), Cordilleran metamorphic core complexes, *Mem. Geol. Soc. Am., 153*, 490 pp., 1980.

Davis, G. A., and G. S. Lister, Detachment faulting in continental extension; perspectives from the Southwestern U.S. Cordillera, *Spec. Pap. Geol. Soc. Am., 218*, 133-159, 1988.

Eaton, G. P., R. R. Wahl, H. J. Protska, D. R. Mabey, and M. D. Kleinkopf, Regional gravity and tectonic patterns: Their relation to late Cenozoic epeirogeny and lateral spreading in the western Corillera, in Cenozoic Tectonics and Regional Geophysics of the Western Cordillera, edited by R. B. Smith and G. P. Eaton, *Mem. Geol. Soc. Am., 152*, 51-92, 1978.

England, P. C., Comment on "Brittle failure in the upper mantle during extension of continental lithosphere" by Dale S. Sawyer, *J. Geophys. Res., 91*, 10487-10490, 1986.

England, P. C., and D. P. McKenzie, A thin viscous sheet model for continental deformation, *Geophys. J. R. astron. Soc., 70*, 295-321, 1982.

Frost, E. G., Structural style of detachment faulting in the Whipple Mountains, California, and Buckskin Mountains, Arizona, *Ariz. Geol. Soc. Dig., 13*, 25-39, 1981.

Hauser, E., C. Potter, T. Hauge, S. Burgess, B. Burtch, J. Mutschler, R. Allmendinger, L. Brown, S. Kaufman, and J. Oliver, Crustal structure of eastern Nevada from COCORP deep seismic reflection data, *Geol. Soc. Am. Bull., 99*, 833-844, 1987.

Howard, K. A., P. Stone, M. A. Pernokas, and R. F. Marvin, Geologic and geochronologic reconnaissance of the Turtle Mountains area, California: West border of the Whipple Mountains detachment terrain, in *Mesozoic-Cenozoic Tectonic Evolution of the Colorado River Region, California, Arizona, and Nevada*, edited by E. G. Frost and D. L. Martin, pp. 341-355, Cordilleran, San Diego, Calif., 1982a.

Howard, K. A., J. W. Goodge, and B. E. John, Detached crystaline rocks of the Mohave, Buck, and Bill Williams Mountains, western Arizona, in *Mesozoic-Cenozoic Tectonic Evolution of the Colorado River Region, California, Arizona, and Nevada*, edited by E. G. Frost and D. L. Martin, pp. 377-390, Cordilleran, San Diego, Calif., 1982b.

Howard, K. A., B. E. John, and C. F. Miller, Metamorphic core complexes, Mesozoic dutile thrusts, and Cenozoic detachments: Old Woman Mountains-Chemehuevi Mountains transect, California and Arizona, in Geologic Diversity of Arizona and Its Margins: Excursions to Choice Areas, edited by G. H. Davis and E. M. VanderDoler, pp. 365-382, Ariz. Bur. of Geol. and Miner. Technol., Tucson, *Spec. Pap. 5*, 1987.

Jackson, J. A., Active normal faulting and crustal extension, in Continental Extensional Tectonics, edited by M. P. Coward, J. F. Dewey, and P. L. Hancock, *Geol. Soc. Spec. Publ. London, 28*, 3-17, 1987.

John, B. E., Geometry and evolution of the midcrustal extensional fault system; Chemehuevi Mountains, southeastern California, in Continental Extensional Tectonics, edited by M. P. Coward, J. F. Dewey, and P. L. Hancock, *Geol. Soc. Spec. Publ. London, 28*, 313-335, 1987.

Jones, C. H., Is extension in the Death Valley accommodated by thinning of the mantle lithosphere beneath the Sierra Nevada, California ?, *Tectonics, 6*, 449-473, 1987.

King, G., and M. Ellis, The origin of large local uplift in extensional regions, *Nature, 348*, 689-693, 1990.

Klemperer, S. L., T. A. Hauge, E. C. Houser, J. E. Oliver, and C. J. Potter, The Moho in the northern Basin and Range province, Nevada, along the COCORP 40°N seismic-reflection transect, *Geol. Soc. Am. Bull., 97*, 603-618, 1986.

Kruse, S., M. McNutt, J. Phippe-Morgan, L. Royden, and B. Wenicke, Lithospheric extension near Lake Mead, Nevada: A model for ductile flow in the lower crust, *J. Geophys. Res., 96*, 4435-4456, 1991.

Melosh, H. J., Mechanical basis for low-angle normal faulting in the Basin and Range province, *Nature, 343*, 331-335, 1990.

Miller, E. L., P. B. Gans, and J. Garing, The Snake Range decollement: An exhumed mid-Tertiary ductile-brittle transition, *Tectonics, 2*, 239-263, 1983.

Moore, R. T., Geology of the Virgin and Beaver Dam mountains, Arizona, *Bull. Ariz. Bur. Mines, 186*, 1-65, 1972.

Olsen, K. H., G. R. Keller, and J. N. Stewart, Crustal structure along the Rio Grande rift from seismic refraction profiles, in Rio Grande Rift: Tectonics and Magmatism, edited by R. E. Riecker, pp. 127-144, AGU, Washington, DC., 1979.

Peltier, W. R., and J. T. Andrews, Glacial-isostatic adjustment, I, The forward problem, *Geophys. J. R. astron. Soc., 46*, 605-646, 1976.

Prodehl, C., and P.W. Lipman, Crustal structure of the Rocky Mountain region, in Geophysical Framework of the Continental United States, edited by L.C. Pakiser and

W.D. Mooney, *Mem. Geol. Soc. Am., 172*, 249-284, 1989.

Reynolds, S. J., and J. E. Spencer, Evidence for large-scale transport on the Bullard detachment fault, west-central Arizona, *Geology, 13*, 353-356, 1985.

Smith, E. I., R. E. Anderson, R. G. Bohannon, and G. J. Axen, Miocene extension, volcanism, and sedimentation in the eastern Basin and Range province, southern Nevada, in Geologic Diversity of Arizona and Its Margins: Excursions to Choice Areas, edited by G. H. Davis and E. M. VanderDoler, pp. 383-387, Ariz. Bur. of Geol. and Miner. Technol., Tucson, *Spec. Pap. 5*, 1987.

Spencer, J. E., Origin of folds of Tertiary low-angle fault surfaces, southeastern California and western Arizona, in *Mesozoic-Cenozoic Tectonic Evolution of the Colorado River Region, California, Arizona, and Nevada*, edited by E. G. Frost and D. L. Martin, pp. 123-134, Cordilleran, San Diego, Calif., 1982.

Spencer, J. E., Role of tectonic denudation in warping an uplift of low-angle normal faults, *Geology, 12*, 95-98, 1984.

Tapponier, P., and P. Molnar, Slip-line theory and large-scale continental tectonics, *Nature, 264*, 319-324, 1976.

Turner, J. S., *Buoyancy Effects in Fluids*, Cambridge University Press, New York, 1973.

Vilotte, J. P., M. Daigniére, R. Madariaga, and O. Zienkiewicz, Numerical study of continental collision: Influence of buoyancy forces and an initial stiff inclusion, *Geophys. J. R. Astron. Soc., 84*, 279-310, 1986.

Walcott, R. I., Flexural rigidity, thickness, and viscosity of the lithosphere, *J. Geophys. Res., 75*, 3941-3954, 1970.

Wdowinski, S., and R. J. O'Connell, Deformation of the central Andes (15° – 27°S) Derived from a flow model of subduction zones, *J. Geophys. Res., 96*, 12,245-12,255, 1991.

Wernicke, B., Low-angle normal faults in the Basin and Range province: Nappe tectonics in an extending orogen, *Nature, 291*, 645-648, 1981.

Wernicke, B., Uniform-sense normal simple shear of the continental lithosphere, *Can. J. Earth Sci., 22*, 108-125, 1985.

Wernicke, B., The fluid crustal layer and its implications for continental dynamics, *Geol. Soc. Am. Abstr. Programs, 21*, A81, 1990a.

Wernicke, B., The fluid crustal layer and its implications for continental dynamics, in *Exposed Cross Sections of the Continental Crust*, edited by M. H. Salisbury and D. M. Fountain, pp. 509-544, Kluwer Academic, Boston, Mass., 1990b.

Wernicke, B., and G. J. Axen, On the role of isostasy in the evolution of normal fault systems, *Geology, 16*, 848-851, 1988.

Wernicke, B., and B. C. Burchfiel, Modes of extensional tectonics, *J. Struct. Geol., 2*, 105-115, 1982.

Wernicke, B., J. D. Walker, and M. S. Beaufait, Structural discordance between Neogene detachments and frontal Sevier thrusts, central Mormon Mountains, southern Nevada, *Tectonics, 4*, 213-246, 1985.

Wernicke, B., G. J. Axen, and J. K. Snow, Basin and Range extensional tectonics at the latitude of Las Vegas, Nevada, *Geol. Soc. Am. Bull., 100*, 1738-1757, 1988.

Wernicke, B., J. K. Snow, G. J. Axen, B. C. Burchfiel, K. V. Hodges, J. D. Walker, and P. L. Guth, Extensional tectonics in the Basin and Range province between the southern Sierra Nevada and the Colorado Plateau, Field Trip Guidebook T138, 28th Int. Geol. Congr., Washington DC, 1989.

White, N., and D. McKenzie, Formation of the "steer's head" geometry of sedimentary basins by differential stretching of the crust and mantle, *Geology, 16*, 250-253, 1988.

Zienkiewicz, O. C., *The finite Element Method*, 3rd ed., McGraw-Hill, New York, 1977.

Zienkiewicz, O. C., *The finite Element Method*, vol. 1, 4th ed., McGraw-Hill, New York, 1977.

Zuber, M. T., E. M. Parmentier, and R. C. Fletcher, Extension of continental lithosphere: A model for two scale of Basin and Range deformation, *J. Geophys. Res., 91*, 4826-4838, 1986.

G. Axen, Department of Earth and Planetary Sciences, 20 Oxford street, Cambridge MA 02138.

S. Wdowinski, Institute for Geophysics and Planetary Physics, Scripps Institution of Oceanography, UCSD (A-025), La Jolla, CA, 92093.

(Received July 2, 1990;
revised July 1, 1991;
accepted August 30, 1991.)